THE JOURNAL OF PHYSICAL CHEMISTRY C

Article

pubs.acs.org/JPCC

Photoinduced Br Desorption from CsBr Thin Films Grown on Cu(100)

M. T. E. Halliday,[†] A. G. Joly,[‡] W. P. Hess,[‡] and A. L. Shluger*[,†]

[†]Department of Physics and Astronomy and London Center for Nanotechnology, University College London, Gower Street, London WC1E 6BT, United Kingdom

[‡]Physical Sciences Division, Pacific Northwest National Laboratory, P.O. Box 999, Richland, Washington 99352 United States

ABSTRACT: Thin films of CsBr deposited onto metals such as copper are potential photocathode materials for light sources and other applications. We investigate desorption dynamics of Br atoms from CsBr films grown on insulator (KBr, LiF) and metal (Cu) substrates induced by sub-bandgap 6.4 eV laser pulses. The experimental results demonstrate that the peak kinetic energy of Br atoms desorbed from CsBr/Cu films is much lower than that for the hyperthermal desorption from CsBr/LiF films. Kelvin probe measurements indicate negative charge at the surface following Br desorption from CsBr/Cu films. Our ab initio calculations of excitons at CsBr surfaces demonstrate that this behavior can be explained by an exciton model of desorption including electron trapping at the CsBr surface. Trapped negative charges reduce the energy of surface excitons available for Br desorption. We examine the electron-trapping characteristics of low-coordinated sites at the surface, in particular, divacancies and kink sites. We also provide a model of cation desorption caused by Franck-Hertz excitation of F centers at the surface in the course of irradiation of CsBr/Cu films. These results provide new insights into the mechanisms of photoinduced structural evolution of alkali halide films on metal substrates and activation of metal photocathodes coated with CsBr.

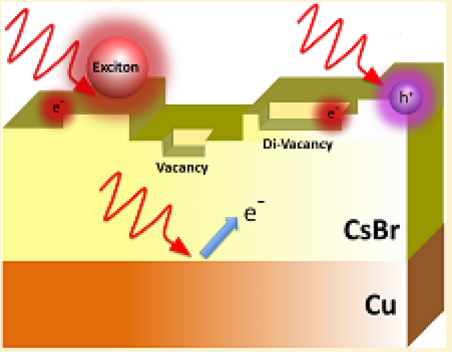

I. INTRODUCTION

Surface electronic excitation is important in many fundamental and applied processes. These include laser desorption and ablation,[1,2] surface photochemistry,[3] selective materials modification,[4,5] photocatalysis, photolithography,[5] and photoemission.[6] Surface excitation of semiconductors and insulators may create both electron−hole pairs and surface excitons, which play a significant role in particle desorption.[7−9] Alkali halides are particularly well studied due to their relatively simple crystalline and electronic structures and sensitivity to ultraviolet light, gamma, X-ray, and particle irradiation. Several mechanisms of photo- and electron-stimulated desorption of alkali halides have been discussed in the literature.[10−17] Electronic structure calculations provide significant insight into the nature of the electronic excited states and desorption mechanisms. Surface excitons are directly involved in halogen-atom desorption.[11−13,18,19] The essential components of the pertinent processes have been established in a series of coupled experimental and theoretical studies.[17−22]

Considerable and related ongoing research is focused on developing new photocathode materials for next-generation synchrotron and free electron laser (FEL) light sources[23] and dynamic and ultrafast transmission electron microscopy (DTEM and UTEM).[24] One promising approach uses thin films of CsBr to modify the surface of metals and substantially increase their photoemission yields.[25] For example, photoemission from Cu substrates coated with a thin CsBr film and then irradiated with an ultraviolet laser light displayed a quantum efficiency (QE) enhancement greater than 50.[25] Maldonado et al. report that a 5 nm CsBr thin film on Nb substrates enhances the QE following activation at 257 nm by a factor of several hundred[26] and significant QE enhancement was also achieved from Cr and Mo photocathodes coated with CsBr.[27,28] Several hours of laser irradiation is necessary to achieve the maximum QE enhancement in a process called laser activation.[25]

Laser activation is primarily associated with photophysics of the alkali halide thin film, although the Cu substrate plays a significant role in the overall process. The first exciton peak of bulk CsBr is 6.96 eV,[29] which is significantly higher than, for example, the 4.66 eV photon energy of the 266 nm YAG fourth harmonic output. Initial photoexcitation therefore proceeds through a two-photon process that deposits 9.32 eV of photon energy, leading to formation of electron hole pairs. Electrons and holes subsequently recombine, in the CsBr thin film, leading to the formation of bulk and surface excitons that then decompose into F and H center defect pairs.[14−18] The subsequent diffusion of H centers to the surface can then lead to desorption of neutral Br atoms, while low-energy photoexcitation of F centers, by visible room light, is thought to cause desorption of Cs atoms. It is possible that some defects are sufficiently metastable to produce a steady-state population of intraband electronic states in the alkali halide thin film.[25−28] Intraband states, such as caused by F centers, could then possibly undergo single photon excitation, leading to electron

Received: August 25, 2015
Revised: September 25, 2015
Published: September 27, 2015

DOI: 10.1021/acs.jpcc.5b08275
J. Phys. Chem. C 2015, 119, 24036−24045

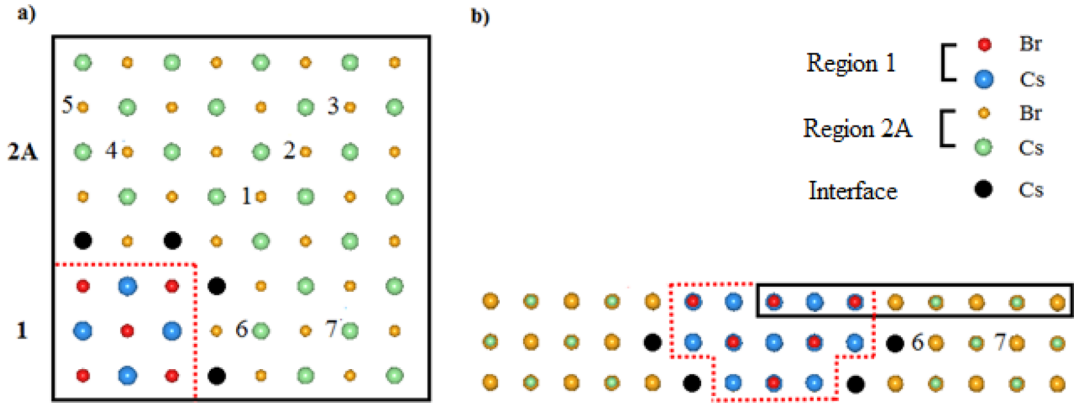

Figure 1. (a) Quadrant of Regions 1 and 2A of the embedding scheme and (b) cross-section of the two regions. Anions and cations are depicted in red and blue in Region 1 and yellow and green in Region 2A, respectively. The interface ions are also included and are colored black. The numbered anions indicate positions where negative charges have been placed, with the resultant desorption energy displayed in Table 1, where atomic labels 6 and 7 designate positions of anions in the bulk. Region 2B and auxiliary point charges are not shown.

photoemission. We note that similar considerations apply for thin films of KBr.

As previously mentioned, the photophysics of alkali halide crystals and thin films, in the absence of a metal substrate, is reasonably well understood under single-photon ultraviolet excitation; however, the presence of a metal substrate can affect the alkali halide photophysics just as dramatically as the presence of the alkali halide thin film alters the photoelectron yield (or QE) of a metal photocathode. Irradiation of a simple CsBr crystal, or thin film grown on an insulating substrate, by 6.4 eV excimer laser pulses produces surface excitons directly. These surface excitons rapidly decompose to desorb neutral Br atoms with hyperthermal kinetic energies and leave behind a surface F center in the newly created vacancy.[9,12,13,30] In the present study we find that thin films of CsBr and KBr on Cu substrates display distinctly different photodesorption properties than do simple single crystals or thin films grown on insulating materials. In particular, the hyperthermal Br atom peak kinetic energy is sharply decreased, from near 0.26 to 0.04 eV in the case of CsBr and from near 0.4 to 0.13 eV for KBr. Surprisingly, we find that the observed kinetic energy reduction does not depend on film thickness, even for films approaching 200 nm. Using a combination of experiment and theory we describe the mechanisms of laser desorption from hybrid metal-alkali halide systems and propose a model that rationalizes the observed effects.

II. METHODS

A. Experimental Methods. The experimental technique and data treatment have been previously described.[11,18] Thin films of CsBr are grown by heating 99.999% pure CsBr powder to 425 °C or KBr powder to 450 °C in an effusion cell whose opening is directed at the face of either a lithium fluoride (LiF) or copper (100) (Cu) substrate. LiF substrates are first heated to 500 °C to remove contaminants. Film growth rates are calibrated using a quartz crystal microbalance positioned at the crystal growth location and orientation. Films of between 7 and 200 nm thickness are then grown using the calibrated rate with the substrate held at room temperature. We estimate the error in the film thickness to be ±5%. The sample is then transported, in vacuum, into the laser desorption chamber, which has a base pressure 4×10^{-9} Torr. The time between film deposition and laser desorption experiments was limited to <1 h to minimize the effects of water adsorption to the extremely hygroscopic CsBr films.

The sample is irradiated using 5 ns excimer laser pulses at 193 nm (6.4 eV) or 157 nm (7.9 eV) and a 10 Hz repetition rate. The desorbed atoms are detected using laser ionization combined with time-of-flight (TOF) mass spectrometry. Laser pulses are directed at the sample at a 60° angle of incidence to the surface normal to induce desorption of neutral bromine atoms. A focused probe laser pulse intersects the desorbed atoms 3.8 mm above and parallel to the sample surface. Tunable light of 5 ns pulse duration from a Nd:YAG pumped frequency-doubled 10 Hz OPO laser tuned to 260.58 nm is used to ionize ground state ($^2P_{3/2}$) bromine atoms in a (2 + 1) REMPI scheme. Atomic masses are determined by a TOF mass spectrometer using chevron microchannel plates to amplify the ion signal. The output signal of the microchannel plates is input to a 500 MHz video amplifier (×10) and then sent to a digital oscilloscope. Data collection is computer-controlled and the lasers can be independently delayed in time using computer interfaced digital delay generators to facilitate measurement of Br($^2P_{3/2}$) yields. Velocity profiles of photodesorbed atoms are determined by integrating the Br-atom yield as a function of the delay between excitation and probe lasers. Velocity profiles are converted to kinetic energy distributions by applying a Jacobian transformation.[31] Each data point represents an average of the integrated mass selected ion signal from 60 laser pulses.

Surface charging was measured utilizing a McCallister Technical Services KP6500 Kelvin probe. The sample surface potential was measured both before and after irradiation with similar laser fluences, as employed in the laser desorption experiments and samples prepared using identical methods. Sample surface charge measurements were performed within 2 min following 266 nm irradiation of between 5 and 15 min and repeated multiple times for consistency. Accumulated surface charge was observed to discharge over the course of several hours.

B. Computational Methods. Both α-CsBr (CsCl-type bcc lattice), and β-CsBr (rocksalt-type fcc lattice) can be grown by choice of a suitable substrate with a favorable lattice parameter (a_0). Previous studies have grown the α-CsBr(110) surface on LiF (a_0 = 4.04 Å) and the β-CsBr(100) surface on KBr (a_0 = 6.60 Å).[30,32] Because the Cu(100) (a_0 = 3.61 Å) surface has a large lattice mismatch (33%) with α-CsBr and a relatively small one (1%) with β-CsBr, we hypothesize that the preferred

DOI: 10.1021/acs.jpcc.5b08275
J. Phys. Chem. C 2015, 119, 24036−24045

surface after growth is β-CsBr (100). We note that low-energy electron diffraction[32] shows that β-CsBr (100) is grown on KBr (lattice mismatch 22 and 8.5% for α- and β-CsBr films, respectively). Therefore, we assume that favorable lattice mismatch will direct the β-CsBr (100) growth on Cu(100) as well and that Cu/KBr and Cu/CsBr samples exhibit the same structures and surfaces. We will focus on CsBr/Cu in the theoretical calculations, assuming that our qualitative results are transferable to Cu/KBr.

The β-CsBr(100) surface was modeled using a QM/MM embedded cluster method, and calculations were performed using the GUESS code.[33] To model the surface, a large 8-layer thick nanocluster of 40 000 points ions of integer charge was constructed, such that the electrostatic potential on the surface is that of a half-infinite crystal to within 1 meV for every ion within 25 Å of the center of the cluster. The details of this procedure are published elsewhere.[34]

The nanocluster is divided into three regions. (See Figure 1.) Region 1 contains atoms described by ab initio DFT methods, with Gaussian basis sets and pseudopotentials used to describe the valence and core electrons, respectively. Region 1 is surrounded by a layer of interface cations, which have large-core pseudopotentials. The interface cations perform the dual role of confining the electron wave functions to Region 1 and act to mediate between the quantum and classical regions. Region 2 is further subdivided into Regions 2A and 2B, where atoms in 2A are described using polarizable, core−shell interatomic potentials by Atwood et al.[35] Region 2A comprises three layers of a square of 225 atoms. (See Figure 1.) Both cores and shells are allowed to move driven by forces. Region 2B consists of fixed, nonpolarizable point ions and comprises all other atoms otherwise not defined.

A modified version of the B3LYP functional[36,37] has been used to describe the electronic structure of Region 1, where the Hartree−Fock exchange-correlation contribution has been raised from the standard 25 to 32.5%. This has been used in previous studies to model excitons and defects in both bulk CsBr[38] and at CsBr surfaces.[30] Small-core Stuttgart pseudopotentials have been used to describe the closed shells of the anions and cations, leaving the $Br^-[(Ar)3s^23p^63d^{10}]4s^24p^6$ and $Cs^+[Ne]4s^24p^65s^0$ electrons to be described by (6s6p1d)/[4s4p1d] and (4s5p1d)/[2s3p1d] basis sets, respectively.[39] All calculations of the ideal surface and defects on the terrace have been conducted with a $Cs_{29}Br_{30}$ quantum cluster. The total energy of Regions 1 and 2 was then minimized until the change in energy per optimization step did not exceed 10^{-5} Hartree.

The Cs−Br separation was calculated as 3.70 Å in Region 1 and 3.68 Å in Region 2. The discrepancy gave rise to a small (<0.25% a_0) increase in the displacement of Region 1 ions in the direction perpendicular to the plane of the surface.

Supplementary calculations of excitons on rough surfaces using a slab model with 2D periodic boundary conditions have also been performed to examine exciton relaxation at low-coordinated surface sites using the CP2K code.[40] They also serve to provide a check on the calculated exciton on the terrace. These calculations have been conducted using the PBE0 functional[41,42] with an increased amount of exact exchange (37.5% instead of 25%), with pseudopotentials on the ions and the relatively large so-called DZVP-MOLOPT double-ζ valence basis sets on the Cs and Br ions.[43] The value of 37.5% exact exchange has been used so as to match the calculated HOMO−LUMO energy difference to the experimental band gap of 7.3 eV, similarly to the B3LYP calculations in the embedding cluster model. This functional is sometimes referred to as PBE38 in the literature, and it is widely used to describe wide band gap insulators (e.g., see refs 44−46).

The unit cell used to model the kink site consisted of four layers of a (5 × 5) surface unit cell (256 ions), with additional atoms placed on the surface forming an incomplete layer, such that there were 297 ions in total, and the nanocorner unit cell consisted of a cube of 216 ions, with 12 Å of vacuum in each direction. The Cs−Br separation in CP2K was calculated as 3.70 Å.

III. RESULTS

A. Experimental Measurements. Figure 2 displays the raw velocity profiles and associated normalized kinetic energy

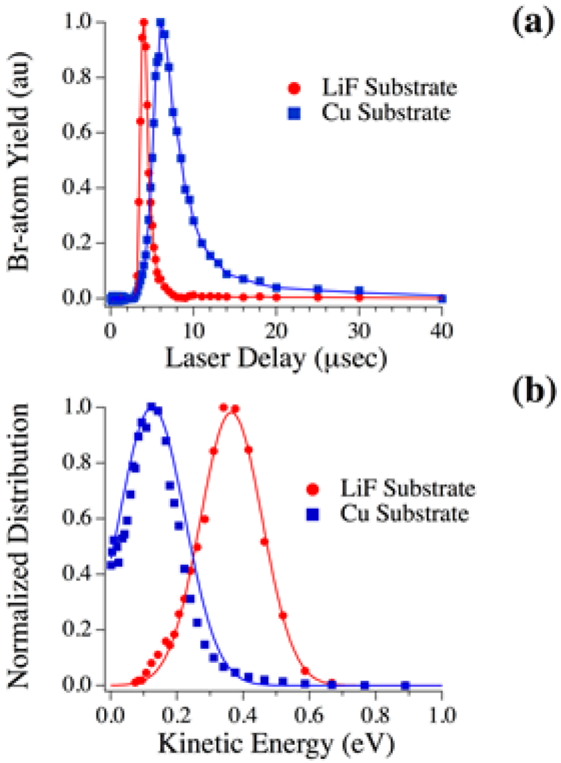

Figure 2. (a) Velocity profiles and (b) associated kinetic energy distribution functions for Br-atom emission from 7 nm KBr films deposited on LiF (red circles) and Cu (blue squares) substrates following 6.4 eV laser excitation.

distributions for $Br(^2P_{3/2})$ emission obtained following 6.4 eV laser photoexcitation of 7 nm KBr films grown on LiF and Cu substrates. The Br-atom velocity profiles (Figure 2a) peak near a laser delay of 4.0 μs for KBr films deposited on LiF, while the peak is near 6 μs for the films deposited on Cu. Figure 2b shows the kinetic energy distributions that result from Jacobian transformation of the velocity data. The KBr/LiF hyperthermal kinetic energy distribution is well fit to a Gaussian with a peak kinetic energy of 0.36 ± 0.002 eV and a width of 0.13 ± 0.003 eV (errors represent one standard deviation). The KBr/LiF hyperthermal kinetic energy distribution is well fit to a Gaussian with a peak kinetic energy of 0.36 eV and a width of 0.13 eV. In contrast, the KBr/Cu kinetic energy distribution peaks near 0.13 eV and has a similar width. The guide line on the KBr/Cu kinetic energy distribution displayed in Figure 2b was obtained by simply translating the fit for the KBr/LiF distribution by

DOI: 10.1021/acs.jpcc.5b08275
J. Phys. Chem. C 2015, 119, 24036−24045

0.235 eV. It is clear that the width of KBr/Cu kinetic energy distribution is slightly smaller than that for KBr/LiF, but otherwise the distribution appears nearly identical though shifted. The decrease in width may be rationalized by realizing that the distribution is necessarily limited on the low energy side because the lowest kinetic energy measurable is near 0 eV. This reduction in symmetry results in an apparent decrease in the distribution width. This suggests that the major effect of the copper substrate is a lowering of the Br-atom kinetic energy by nearly 0.24 eV.

Figure 3 displays the analogous velocity profiles and kinetic energy distributions for Br-atom desorption following 6.4 eV

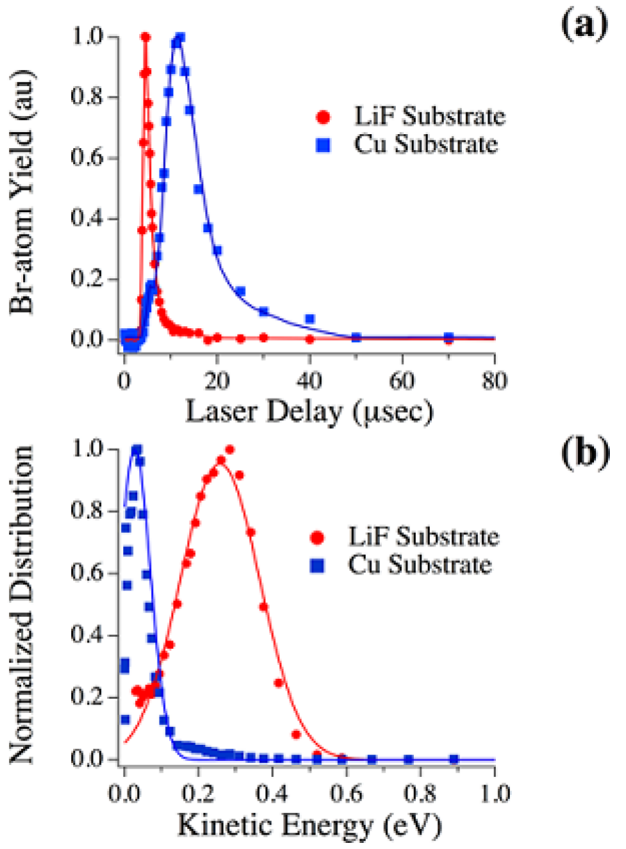

Figure 3. (a) Velocity profiles and (b) associated kinetic energy distribution functions for Br-atom emission from CsBr films deposited on LiF (red circles) and Cu (blue squares) substrates following 6.4 eV laser excitation.

photoexcitation of 7 nm CsBr films grown on both LiF and Cu substrates. The peak of the velocity distribution (Figure 3a) for Br-atom emission from CsBr films on LiF is ~4.6 μs, while for analogous films on copper, the peak is near 12 μs. The transformed kinetic energy distribution for CsBr thin films grown on LiF can be fitted to a Gaussian with peak energy of 0.26 ± 0.003 eV and a width of 0.15 ± 0.004 eV (Figure 3b).The transformed kinetic energy distribution for CsBr thin films grown on LiF can be fitted to a Gaussian with peak energy of 0.26 eV and a width of 0.15 eV (Figure 3b). These values are consistent with a previous report[30] and significantly smaller than the result from the KBr thin films. By analogy to results from KBr films displayed in Figure 2, the guide line on the CsBr/Cu kinetic energy distribution is simply a translation of the CsBr/LiF fit by 0.23 eV, although the width decreases significantly to 0.06 eV. In this case, Br atoms emitted from CsBr films have a significantly smaller maximum energy available; therefore, a reduction of 0.23 eV produces a distribution with a peak much closer to zero kinetic energy and therefore a much more significant change in the observed width as previously outlined for KBr films on copper.

The data displayed in Figures 2 and 3 are from nominally 7 nm thick films, but we have performed identical measurements on films ranging between 3 and 200 nm in thickness. Figure 4

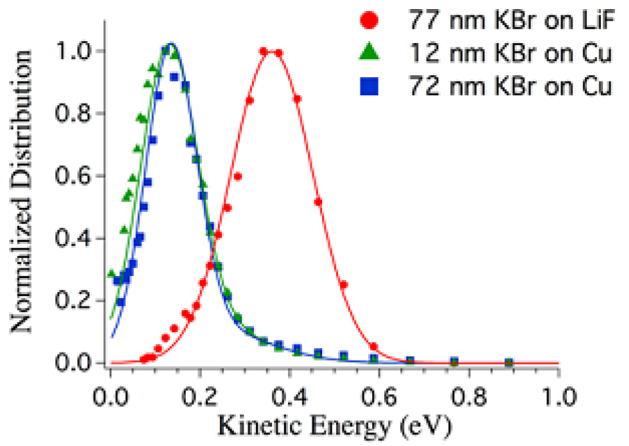

Figure 4. Kinetic energy distribution functions for Br-atom emission from 77 nm thick KBr films deposited on LiF (red circles) and a 12 nm thick KBr film deposited on Cu (blue squares) and a 72 nm thick KBr film deposited on Cu (green triangles) following 6.4 eV laser excitation. The nominal film thickness does not appreciably change the recorded kinetic energy distribution function.

displays results from both a thick (72 nm) and thin (12 nm) KBr film grown on Cu as well as a thick (77 nm) KBr film grown on LiF for comparison. The general result is that the kinetic energy distributions and, in particular, the peak kinetic energies for the films grown on Cu, do not change appreciably over these thickness ranges, within a kinetic energy error range of ±0.02 eV. In addition, the peak kinetic energy of the 77 nm-thick KBr film is nearly identical with the thin (7 nm thick) film displayed in Figure 2 and is consistent with single-crystal KBr results.[11] Thickness-dependent results on CsBr films grown on copper up to nominal 200 nm thickness show similar results, where the kinetic energy distributions do not depend significantly on film thickness.

Kelvin probe experiments conducted ~2 min after irradiation measure a small negative potential at the surface of −0.15 V, which is equivalent to a charge density of ~10^6 electron/cm^2.

B. Theoretical Calculations. *Theoretical Model.* Theoretical models of Br-atom desorption from the α-CsBr (CsCl-type lattice) and β-CsBr (rocksalt-type lattice) surfaces induced by 6.4 and 7.9 eV ns laser pulses have been discussed in ref 30. The experimental band gap of β-CsBr is 7.3 eV,[47] and the first singlet exciton peak occurs at 6.96 eV.[29] The position of the surface exciton peak is not established experimentally, but our calculations predict it at ~6.4 eV.[30] This suggests that 6.4 eV photons can excite surface excitons but are unlikely to excite bulk excitons.

The main mechanisms by which 6.4 eV photons interact with the Cu/CsBr system are schematically depicted in Figure 5. The process (1) corresponds to photons creating excitons at the surface. Excitons on the terrace can relax by desorbing a Br atom, which has been established to be the primary source of desorbed Br atoms from CsBr grown on insulating surfaces.[30]

DOI: 10.1021/acs.jpcc.5b08275
J. Phys. Chem. C 2015, 119, 24036−24045

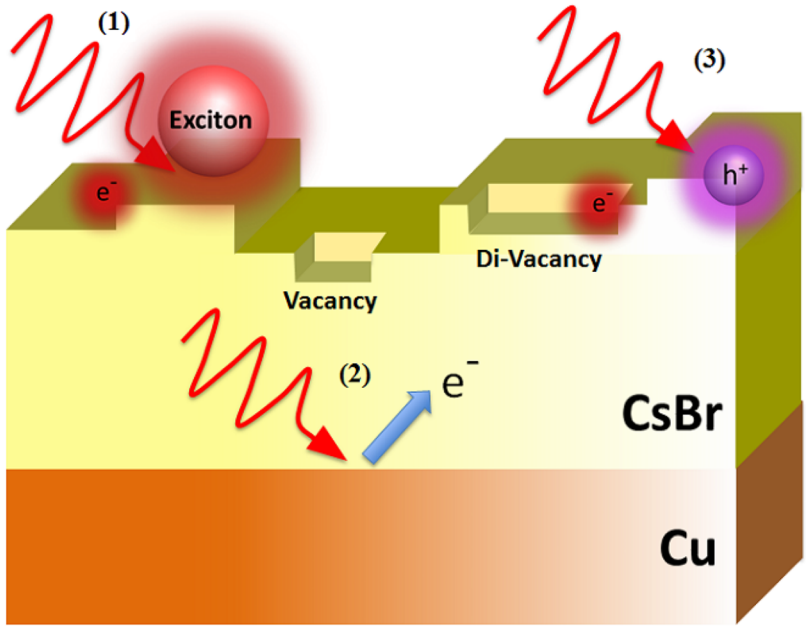

Figure 5. Three ways of interaction for incident photons. Radiation will: (1) create excitons on the surface, either at the terrace or at low-coordinated sites; (2) penetrate the film and induce photoemission of electrons from the Cu substrate; and (3) ionize low-coordinated sites at the surface, leaving trapped holes, which may then lead to desorption.

In contrast with CsBr films grown on an insulating substrate, photons penetrating the CsBr films grown on Cu induce photoemission of electrons from Cu, as (2). A study of photoemission following irradiation of Cu at 6.2 eV indicates a wide distribution of electron kinetic energies ranging from 0 to 2 eV, peaking at ∼1 eV.[48] A previous study has measured a reduction of the work function of bare Cu after the application of a 7 nm CsBr film from 4.2 to 3.4 eV.[49] This would increase the mean of electron distribution energies to 1.8 eV, with photoemitted electrons of 2.8 eV at the high-velocity end of the distribution. Previous studies also suggest that electrons at these energies have a large mean free path in CsBr.[49−51] We can expect some of the electrons passing through CsBr to the surface to either become trapped by defects or low-coordinated surface sites or to excite defects. Finally, as (3), incoming photons can ionize low-coordinated sites, and the Br atom on which a hole is localized can become more loosely bound to the surface and subsequently desorb. Irradiated CsBr films grown on LiF can induce desorption by pathways (1) and (3); however, desorption from CsBr/Cu is affected by electrons photoemitted as (2). Therefore, one of the reasons for the difference between the desorbed Br velocity distributions could be due to the presence of these electrons. Another reason could be related to the difference in morphology of CsBr surfaces for films grown on LiF and Cu. Below we undertake an analysis of several desorption pathways.

Exciton Decomposition at the (100) Surface of β-CsBr. An excitonic mechanism of irradiation-induced halogen atom desorption from alkali halide surfaces has been discussed in a series of papers[12,13,17−22] and summarized in a review.[52] It is based on the idea that surface excitation can initially lead to the formation of a localized one-center triplet exciton, which can relax by desorbing a halogen atom (so-called hyperthermal desorption) or by forming a surface self-trapped exciton. The latter can either recombine and thus restore the perfect lattice or produce a pair of Frenkel defects, a neutral halogen vacancy, and interstitial halogen atom. The excitonic mechanism describes the desorption of alkali halides and has been shown to explain the experimental data on Br desorption from the α-CsBr and β-CsBr surfaces.[30] Therefore, we assume that the difference in peak kinetic energy of Br atoms desorbing from CsBr/Cu with respect to CsBr/LiF could be caused by some perturbation of surface exciton state and start our calculations from modeling surface excitons.

After singlet excitation, excitons in alkali halides are known to quickly convert into the lower triplet state.[53,54] The triplet excited state of CsBr surface can be modeled using ground-state DFT methods, as the lowest energy triplet state corresponds to the promotion of an electron from the valence band into the conduction band. In both QM/MM and periodic calculations, the triplet state of the perfect surface has both the excited electron and the hole fully delocalized by the surface ions. The exciton localization on a particular surface ion results from small thermal fluctuation. By pulling Br ion out of the surface by 0.1 Å (∼2%a_0), within vibrational displacements of surface anions at room temperature, we model a Frenkel-type one-center exciton localized on the surface before full relaxation has occurred. The classical shells in Region 2A are allowed to relax to correctly simulate charge screening effects. To examine the electron density distribution we have used the so-called natural population analysis technique to assign electronic density to orbitals about ionic centers, described in more detail here.[55] A natural population analysis of the exciton shows 0.4|e| of the hole in the protruding Br 4p orbital polarized perpendicular to the surface, with 0.5|e| contributions from the four nearest neighbor Br 4p orbitals. The electron component is more diffuse, appearing to bulb out of the surface, with 0.35|e| and 0.2|e| in the four nearest neighbor Cs 6s and 6p orbitals, respectively. The remaining electron density is spread across the Cs 6s orbitals of the cluster. This exciton state is described in more detail in ref 30.

Br desorption energy is defined as the energy difference between the unrelaxed exciton (initial state) and an F center at the surface and a Br atom at infinite separation (final state).

DOI: 10.1021/acs.jpcc.5b08275
J. Phys. Chem. C 2015, 119, 24036−24045

Positive values mean that the Br atoms have an extra energy equal to the upper limit of kinetic energy available. The part of this energy lost to exciton relaxation and phonons during desorption process is not calculated here. We have checked that there is no energy barrier for Br desorption via this mechanism.

F centers on the surface have been modeled by removing an anion and replacing it with a "ghost" basis set equal to that on the Br anions at the vacancy site. The ionic coordinates of all atoms in Regions 1 and 2A are then allowed to relax driven by forces until the energy is minimized. The electron trapped at the surface F center has an energy level 1.7 eV below the vacuum level. A natural population analysis shows 0.1|e| described by the vacancy s orbitals, 0.7|e| by the neighboring Cs 6s orbitals, and the remainder consisting of contributions from the Cs 5d orbitals. The calculated maximum kinetic energy of Br atom is 0.65 eV, in good agreement with a previous study[30] using periodic boundary conditions, which predicted 0.66 eV and with the results presented in Figure 3.

These results confirm that 6.4 eV photon excitation can cause desorption of Br atoms with hyperthermal velocities from CsBr surface terraces. This means that the surface will evolve during repeating laser pulses. To understand better the character of this evolution we investigate the desorption of Cs atoms.

Cs Atom Desorption and Formation of Divacancies. Although anion desorption caused by surface excitation of the alkali halides is well studied, cation desorption is much less understood and the experimental data are scarce. Almost equal depletion of Cs and Br has been observed in the XPS spectra of thick CsBr/Cu films irradiated by UV (266 nm) light,[49] and AFM images of electron bombarded KBr show that stoichiometry is largely preserved and the surface evolves via the formation and expansion of rectangular pits.[56] Emission of ground-state Na atoms has been observed from NaCl samples after an optical excitation of electron-irradiated samples.[57] The theoretical calculations suggested that Na desorption from NaCl may be due to electronically *excited* F centers (F*), although the calculations using the Hartree−Fock methods predicted a substantial barrier to this process (2.1 eV).[58]

The calculated energy difference between the perfect surface and a surface with a neutral cation vacancy and a Cs atom at infinite separation is 6.0 eV. The difference in energy between an F center at the surface and a divacancy and Cs atom at infinite separation is significantly reduced, at 1.3 eV, but still too large to expect spontaneous emission.

To investigate the mechanism proposed in ref 58, we have pulled the Cs atom from the surface and calculated the adiabatic potential energy surface (APES) for three different scenarios: (a) desorption from a terrace site; (b) desorption from a site adjacent to an F center; and (c) desorption from a site adjacent to an electronically excited F center, F*. In the latter case, the calculations were carried out using time-dependent (TD)-DFT for each position of the Cs ion. The excited F-center orbital is initially delocalized on the four neighboring Cs ions. After pulling a neighboring Cs ion out of the surface by a value of 0.01 Å, within thermal vibrational amplitudes at room temperature, the lowest energy transition involves excitation of the F-center electron onto the Cs^+ ion protruding from the surface, forming a neutral Cs atom. The energy surface is flat up to 1.25 Å from the surface, and the difference in energy between F* state and a divacancy and Cs atom at infinite separation is calculated as 0.08 eV (Cs atom desorption energy). These calculations predict Cs atoms desorb at lower energies than Br atoms. We checked that Cs atoms prefer to desorb perpendicular to the (100) surface in all three cases. The initial excitation energy of the F center on the surface is calculated as 2.14 eV, well within the energies available to photoemitted electrons.

These results suggest that Cs desorption from the sites adjacent to excited F centers is feasible and could lead to the formation of divacancies. Surface F centers can be excited by hot electrons photoemitted from the Cu substrate and traveling in the CsBr conduction band, an analogue of the so-called Franck-Hertz effect in solids.[59] The excitation of F-center electrons by electrons in the conduction band in Al_2O_3 has been extensively studied,[60] as has the luminescence behavior of electron-excited Ag^+ and Tl^+ impurity ions in similar alkali halides such as RbCl and KCl.[61,62]

Alternative Br Desorption Pathways. To provide a comprehensive analysis of other potential pathways, which may contribute to Br desorption, we examined also exciton creation at low-coordinated sites, excited states of surface defects induced by photoemitted electrons, and the possibility of desorption via hole creation at low-coordinated sites corresponding to processes (1)−(3) in Figure 5.

Apart from interacting with surface terraces, 6.4 eV photons may create excitons at nanocorner and kink sites. To examine if these excitons can contribute to the desorbed Br distribution, excitons and F centers have been modeled at nanocorner and kink sites. In contrast with all other calculations in this study, which use the embedding cluster scheme, the periodic model implemented in the CP2K code has been used to calculate these defects as computation is relatively efficient, and the defects are neutral. The resulting desorption energy has been calculated as 0.70, 0.30, and 0.38 eV on the terrace, nanocorner, and kink sites, respectively. The decrease in energy is largely due to the exciton being of lower energy. The calculation of the APES for Br atom desorption perpendicular to the surface plane shows the energy monotonically decreases in all cases, indicating that there are no barriers to these processes. We note that the cross-section of photon interaction with the terrace will be much larger than that with nanocorner and kink sites, as there are significantly more terrace sites. Nevertheless, part of the low-energy desorbed Br atoms can originate from exciton relaxation at these low-coordinated sites.

Photoemitted electrons from the Cu substrate, as (2) in Figure 5, can interact with existing defects at the surface, which can potentially contribute toward atomic desorption. In particular, as previously shown, electrons can excite F centers, leading to cation desorption. Excitons may also be created at surface divacancy sites. To establish whether the relaxation of excited divacancies can contribute to the Br desorption, we calculated the energy difference between the initial exciton state and a trivacancy and Br atom at infinite separation. An exciton at a divacancy has been calculated by promoting the system into a triplet state. The trivacancy, with two neighboring anion vacancies, has also been calculated; however, the final state is higher in energy by 0.6 eV, suggesting that this mechanism cannot contribute to the desorption process.

Finally, we examined whether ionization of Br corner and kink sites, as process (3) in Figure 5, could subsequently lead to Br atom desorption. The ionization energies of the kink and nanocorner sites are 5.9 and 6.2 eV, respectively, and they can be ionized by incoming 6.4 eV photons. This leads to the formation of trapped holes, essentially Br atoms at these sites. Although this leads to a significant reduction of bonding of Br

DOI: 10.1021/acs.jpcc.5b08275
J. Phys. Chem. C 2015, 119, 24036−24045

atoms with the surface, the barriers for Br atom desorption are 0.7 and 0.6 eV, for the kink and nanocorner sites, respectively. Therefore, we conclude that thermally activated desorption via this mechanism is possible but comparatively insignificant with respect to exciton-induced desorption.

Effect of Negative Surface Charging on Br Desorption. The Kelvin probe measurement indicates that a small negative charge is present on the CsBr surface after irradiation, suggesting that charges at the surface may be playing a role in reducing the energy available for desorbing Br atoms. The embedded cluster method allows the addition of charge in Region 2 while leaving the spin state of Region 1 unchanged, such that we can study the triplet exciton using DFT in the presence of extra electrons. The effect of trapped electrons/holes at the surface was simulated by changing the charge of the classical shells in Region 2A at sites labeled in Figure 1 and recalculating the exciton and F-center electronic structures. Charges have also been placed in the layers immediately below the surface. The shells of Region 2A are allowed to relax, with all other coordinates fixed.

The Br kinetic energies for different positions of single negative charge at the surface are given in Table 1, along with the corresponding distance to the center of the cluster where an exciton is localized. Positive charges were found to increase the available energy and have not been further investigated.

Table 1. Calculated Desorption Energy (E_D) with Negative Charges at Positions Indicated in Figure 1, with the Corresponding Distances between the Charge and Exciton (r)

position	r (Å)	E_D (eV)
1	15.7	0.34
2	20.8	0.50
3	26.0	0.58
4	14.8	0.50
5	13.3	0.48
6	18.8	0.45
7	31.2	0.57
no charge		0.66

We note that the presence of negative charge reduces the kinetic energy by as much as 0.3 eV. The surface F-center formation energy is calculated as 5.30 eV in all cases, except when the charge is placed at position 1, where it decreases slightly to 5.18 eV.

The effect of the negative charge on the electron component of the exciton is relatively small, with the bulk of the difference in energy due to the raising of the hole energy level. The hole energy level rises by 0.5 eV as the charge is moved from position 1 to position 3, and rises by 1 eV with the charge at position 1 with respect to the uncharged surface. We note that the local environment of charges at positions 1, 2, and 3 is characterized by a line of anions between the charge and the exciton, whereas charges at positions 4 and 5 are separated from the exciton by both anions and cations. The difference in polarizability of the Br^- and Cs^+ ions (approximately 6 and 2.4 $Å^3$, respectively[63]) and their consequent screening accounts for the difference in desorption energy for charges at similar distances from the exciton but at different positions (e.g., 1 and 5).

These results suggest that electrons trapped at the surface can affect exciton states and reduce kinetic energies of desorbing Br atoms; however, to induce the observed shift the concentration of electron trapping sites should be high, approximately 1 in 100 atoms. Later we investigate possible electron trapping sites at the CsBr surface.

Electron Trapping Sites at the β-CsBr (100) Surface. Electrons can be trapped in the bulk at grain boundaries and dislocations.[64] F centers in bulk CsBr can also trap electrons,[38,65] and become F^- centers. The additional electron raises the energy of the state due to the Coulomb repulsion between the two electrons, and the occupied energy level rises in energy. The F center has been calculated previously as being lower in energy than the F^- center in the bulk by 1.0 eV.[38] The one-electron energy levels of the F center and F^- center in the bulk have been calculated as being 2.7 and 0.5 eV below the conduction band, respectively.[38]

In Table 2 we summarize the results for electron interaction with several surface sites. We calculate vertical electron affinities (EAs), which characterize the electron trapping cross-section; vertical ionization potential (IP) after the full relaxation of the negatively charged defect, which characterizes the depth of the potential well; and thermal ionization energy of the extra electron (ΔE), the difference in total energies between the fully relaxed states with and without an extra electron.

Table 2. Results for the Calculated EA, IP, and ΔE of Each Trapping Site, Where a Positive Number for ΔE Indicates That the System with an Extra Electron Is of Lower Energy than without the Electron

	EA (eV)	IP (eV)	ΔE (eV)
terrace	−0.66		
F center	−0.35	0.30	−0.13
divacancy	−0.22	0.85	0.28
trivacancy	−0.30	0.47	0.05
quad-vacancy	−0.47	0.22	−0.12
step	−0.03	0.14	0.08
kink	0.01	0.45	0.23
nanocorner	−0.13	0.23	0.08

F centers will be dynamically produced on the surface as products of desorption. The vertical electron affinity (EA) of F centers at the surface is calculated as −0.35 eV, although after relaxation into an F^- center the IP is calculated as 0.3 eV. The cations and anions relax toward and away from the defect, respectively. The F and F^- centers are depicted in Figure 6a,b, along with the geometric relaxation induced by the electron. A natural population analysis of the F^- center shows 1.6|e| and 0.2|e| described by the four neighboring Cs 6s and 6p orbitals, respectively, with 0.2|e| on the Cs 6s orbital immediately below the surface defect and almost no electron density described by the vacancy basis. Because there is an energy cost associated with the initial capture of an electron and the IP is small, we expect F centers to act as transient electron traps, although it seems unlikely that such shallow traps can account for all of the negative charge that our calculations and experiment predict to be at or around the surface.

The divacancy has been calculated as having a vertical EA of −0.22 eV, but after relaxation of the surrounding ions the IP is calculated as 0.85 eV. The bulk of the electron density is in the anion vacancy, with some density spilling over into the vacant cation site. The HOMO iso-surfaces and the local geometric relaxation of the F center and divacancy with and without a trapped electron are depicted in Figure 6c,d.

DOI: 10.1021/acs.jpcc.5b08275
J. Phys. Chem. C 2015, 119, 24036−24045

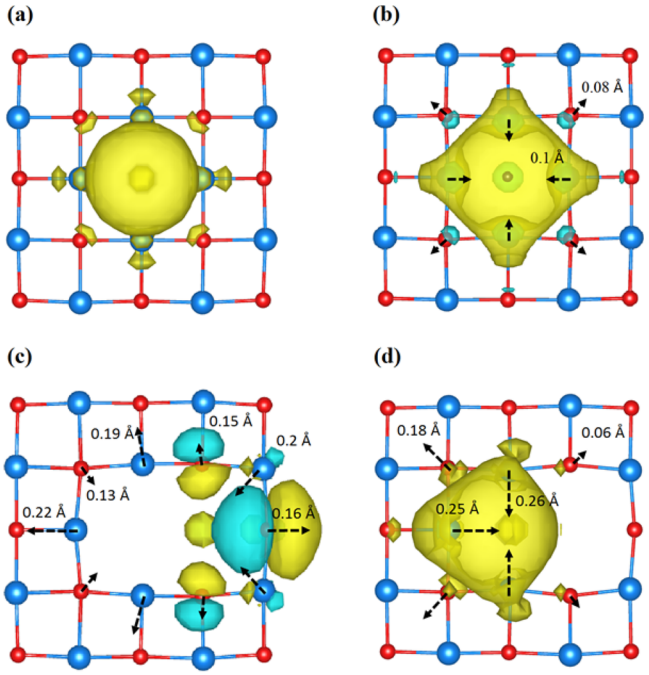

Figure 6. Iso-surfaces of the HOMO of (a) an F center, (b) an F^- center, (c) a divacancy, and (d) a divacancy with a trapped electron. The geometric relaxation is given with respect to the defectless surface for (c) and with respect to the neutral defects (i.e., (a) and (c), respectively) for (b) and (d), with the length of the arrow corresponding to the magnitude of displacement in the directions indicated.

In contrast with F centers, divacancies are deep electron traps, and should contribute to the negative charge at the surface. We undertake here an examination of other potential trapping sites at the CsBr surface.

Both trivacancies and quad-vacancy pits have been calculated to determine their electron-trapping characteristics. Step, nanocorner, and kink sites have also been examined as potential electron trapping sites. The results are summarized in Table 2.

The electron trapped at the trivacancy (two neighboring anion vacancies and an adjoining cation vacancy) occupies an orbital primarily distributed over the two anion vacancies and in equal proportion. The negative charge induces relaxation of neighboring cations toward the void. This lowers the electrostatic potential at the two anion vacancy sites such that the occupied energy level rises and the electron affinity decreases. This effect increases with the pair of adjacent divacancies, or quad-vacancy, where the electron is sitting in a similar orbital with a higher energy level again.

These results demonstrate that divacancies, corner, and kink sites are the most likely electron traps at the surface. The calculated density of surface negative charge required to reduce the peak kinetic energy of desorbing Br atoms by 0.2 to 0.3 eV corresponds to approximately one electron trapped per (13×13) atomic surface units, which is equivalent to a charge density of 4×10^{12} electrons/cm^2. On the contrary, the Kelvin Probe measurement of the charge at the surface at room temperature ~2 min after irradiation reveals a small negative charge of $\sim 10^6$ electron/cm^2. The difference in charge density can be explained by the results presented in Table 2. We can expect electrons to escape shallow potential wells thermally, for which the third column of Table 2, the difference in energy between the depths of the potential well with and without an electron (ΔE), acts as a lower bound. All examined trapping sites have thermal ionization energies under 0.3 eV. After 2 min we would expect the vast majority of these sites to discharge, with any remaining charge likely to be trapped at divacancies or kink sites.

IV. CONCLUSIONS

We have presented the results for photoinduced desorption from KBr and CsBr films grown on an insulator and metal substrates. The kinetic energy distributions of emitted Br atoms change from a single narrow peak for film on an insulator to a distribution that peaks at a lower energy with a high energy tail on the metal substrate. The lack of dependence on the thickness of the KBr and CsBr films suggests that this difference is not due to direct interaction between the metal and the KBr or CsBr surface. The results of ab initio calculations suggest that the difference in the photophysics of CsBr films grown on an insulator and a metal can be explained by trapping of electrons photoemitted from Cu at low-coordinated sites and vacancy clusters at the CsBr surface. In a dynamic process of electron escape and replenishment by new photoemitted electrons on an evolving surface, these electrons affect the energies of surface triplet excitons. Previous experiments by Bennewitz et al.[56] reveal a layer-by-layer desorption of KBr induced by 1 keV electron bombardment through the formation of expanding pits with increased number of kink sites. We assume that the photoexcited surface of CsBr undergoes similar transformation. Our results provide new insights into the mechanisms of photoinduced structural evolution of alkali halide films on metal substrates and activation of metal photocathodes coated with CsBr.

AUTHOR INFORMATION

Corresponding Author

*E-mail: a.shluger@ucl.ac.uk. Phone: +44 (0)20 7679 1312.

Notes

The authors declare no competing financial interest.

ACKNOWLEDGMENTS

M.T.E.H. is grateful to EPSRC for financial support. We acknowledge support from the U.S. Department of Energy (DOE), Office of Basic Energy Sciences, Division of Chemical Sciences, Geosciences & Biosciences. A portion of this work was performed using EMSL, a national scientific user facility sponsored by DOE's Office of Biological and Environmental Research and located at PNNL. PNNL is a multiprogram national laboratory operated for DOE by Battelle. Access to the Archer facility is provided via our membership of the U.K.'s HPC Materials Chemistry Consortium, which is funded by EPSRC grant EP/F067496.

REFERENCES

(1) Al-Shamery, K.; Freund, H.-J. *Proceedings of the 11th International Workshop on Desorption Induced by Electronic Transitions*; Elsevier: Amsterdam, 2008; and preceding volumes in this series.

(2) Hess, W. P.; Herman, P. R.; Bauerle, D.; Koinuma, H. *Journal of Physics: Conference Series Vol. 59*; IOP Publishing, Bristol and Philadelphia, 2005; and preceding volumes in this series.

(3) Zhu, X.-Y. Surface Photochemistry. *Annu. Rev. Phys. Chem.* **1994**, *45*, 113−144.

(4) Kanasaki, J.; Iwata, K.; Tanimura, K. Translational Energy Distribution of Si Atoms Desorbed by Laser-Induced Electronic Bond

DOI: 10.1021/acs.jpcc.5b08275
J. Phys. Chem. C 2015, 119, 24036−24045

Breaking of Adatoms on Si(111)-(7 × 7). *Phys. Rev. Lett.* **1999**, *82*, 644−647.
(5) Stoneham, A. M.; Itoh, N. *Materials Modification by Electronic Excitation*; Cambridge University Press: Cambridge, U.K., 2000.
(6) Huefner, S. *Photoelectron Spectroscopy*, 3rd ed.; Springer Series in Solid State Physics; Springer-Verlag: Berlin, 2003.
(7) Elliott, D. J.; Townsend, P. D. Defect Formation and Sputtering of Alkali Halides with Low Energy Irradiation. *Philos. Mag.* **1971**, *23*, 249−259.
(8) Schmid, A.; Braeunlich, P.; Rol, P. K. Multiphoton-Induced Directional Emission of Halogen Atoms from Alkali Halides. *Phys. Rev. Lett.* **1975**, *35*, 1382−1385.
(9) Smoluchowski, R. Mechanism of Emission of Halogen Atoms from Alkali Halides. *Phys. Rev. Lett.* **1975**, *35*, 1385−1387.
(10) Szymonski, M. Electronic Sputtering of Alkali Halides. *J. Phys.: Condens. Matter* **1993**, *43*, 495−526.
(11) Beck, K. M.; Joly, A. G.; Hess, W. P. Evidence for a Surface Exciton in KBr via Laser Desorption. *Phys. Rev. B: Condens. Matter Mater. Phys.* **2001**, *63*, 125423−125432.
(12) Puchin, V. E.; Shluger, A. L.; Itoh, N. Theoretical Studies of Atomic Emission and Defect Formation by Electronic Electronic Excitation at the (100) Surface of NaCl. *Phys. Rev. B: Condens. Matter Mater. Phys.* **1993**, *47*, 10760−10768.
(13) Puchin, V.; Shluger, A.; Nakai, Y.; Itoh, N. Theoretical Study of Na-atom Emission from NaCl (100) Surfaces. *Phys. Rev. B: Condens. Matter Mater. Phys.* **1994**, *49*, 11364−11373.
(14) Kolodziej, J.; Szymonski, M. Hot-carrier Transport Processes in Stimulated Desorption of Alkali Halides. *Phys. Rev. B: Condens. Matter Mater. Phys.* **1998**, *58*, 13204−13211.
(15) Fu, C. R.; Chen, L. F.; Song, K. S. Decay of Self-trapped Exciton near the (001) Surface in NaBr and KBr. *J. Phys.: Condens. Matter* **1999**, *11*, 5699−5704.
(16) Kolodziej, J. J.; Such, B.; Czuba, P.; Krok, F.; Piatkowski, P.; Struski, P.; Szymonski, M.; Bennewitz, R.; Schaer, S.; Meyer, E. Frenkel Defect Interactions at Surfaces of Irradiated Alkali Halides Studied by Non-Contact Atomic-Force Microscopy. *Surf. Sci.* **2001**, *482*, 903−909.
(17) Hess, W. P.; Joly, A. G.; Beck, K. M.; Sushko, P. V.; Shluger, A. L. Determination of Surface Exciton Energies by Velocity Resolved Atomic Desorption. *Surf. Sci.* **2004**, *564*, 62−70.
(18) Hess, W. P.; Joly, A. G.; Gerrity, D. P.; Beck, K. M.; Sushko, P. V.; Shluger, A. L. Selective Laser Desorption of Ionic Surfaces: Resonant Surface Excitation of KBr. *J. Chem. Phys.* **2001**, *115*, 9463−9472.
(19) Hess, W. P.; Joly, A. G.; Gerrity, D. P.; Beck, K. M.; Sushko, P. V.; Shluger, A. L. Control of Laser Desorption Using Tunable Single Pulses and Pulse Pairs. *J. Chem. Phys.* **2002**, *116*, 8144−8151.
(20) Beck, K. M.; Joly, A. G.; Hess, W. P.; Gerrity, D. P.; Dupuis, N. F.; Sushko, P. V.; Shluger, A. L. Transient Center Photodecomposition in Potassium Bromide. *Appl. Surf. Sci.* **2002**, *197*, 581−586.
(21) Henyk, M.; Joly, A. G.; Beck, K. M.; Hess, W. P. Photon Stimulated Desorption from KI: Laser Control of I-atom Velocity Distributions. *Surf. Sci.* **2003**, *528*, 219−223.
(22) Joly, A. G.; Beck, K. M.; Henyk, M.; Hess, W. P.; Sushko, P. V.; Shluger, A. L. Surface Electronic Spectra Detected by Atomic Desorption. *Surf. Sci.* **2003**, *544*, L683−L688.
(23) Cultrera, L. Advances in Photocathodes for Accelerators. In *Proceedings of 5th International Particle Accelerator Conference (IPAC 2014)*; JACoW: Geneva, Switzerland, 2014; p MOZB02.
(24) Dowell, D. H.; Bazarov, I.; Dunham, B.; Harkay, K.; Hernandez-Garcia, C.; Legg, R.; Padmore, H.; Rao, T.; Smedley, J.; Wan, W. Cathode R and D for Future Light Sources. *Nucl. Instrum. Methods Phys. Res., Sect. A* **2010**, *622*, 685−697.
(25) Liu, Z.; Maldonado, J. R.; Dowell, D. H.; Kirby, R. E.; Sun, Y.; Pianetta, P.; Pease, F. Electron Sources Utilizing Thin CsBr Coatings. *Microelectron. Eng.* **2009**, *86*, 529−531.
(26) Maldonado, J. R.; Pianetta, P.; Dowell, D. H.; Smedley, J.; Kneisel, P. Performance of a CsBr Coated Nb Photocathode at Room Temperature. *J. Appl. Phys.* **2010**, *107*, 013106.1−013106.3.
(27) Liu, Z.; Maldonado, J.; Sun, Y.; Pianetta, P.; Pease, R. F. W. CsBr Photocathode at 257 nm: A Rugged High Current Density Electron Source. *Appl. Phys. Lett.* **2006**, *89*, 111114−111126.
(28) Maldonado, J. R.; Coyle, S. T.; Shamoun, B.; Yu, M.; Gesley, M.; Pianetta, P. Cs Halide Photocathode for Multi-Electron-Beam Pattern Generator. *J. Vac. Sci. Technol., B: Microelectron. Process. Phenom.* **2004**, *22*, 3025−3031.
(29) Lipp, M.; Yoo, C.; Strachan, D.; Daniels, W. Band Structure Parameters and Fermi Resonances of Exciton-Polarons in CsI and CsBr under Hydrostatic Pressure. *Phys. Rev. B: Condens. Matter Mater. Phys.* **2006**, *73*, 085121−085128.
(30) Halliday, M. T. E.; Joly, A. G.; Hess, W. P.; Sushko, P. V.; Shluger, A. L. Mechanisms of Photodesorption of Br Atoms form CsBr Surfaces. *J. Phys. Chem. C* **2013**, *117*, 13502−13509.
(31) Auerbach, D. J. In *Atomic and Molecular Beam Methods Vol. 1, Chapter 14*; Scoles, G., Bassi, D., Buck, U., Laine, D. C., Eds.; Oxford University Press: New York, 1988.
(32) Kiguchi, M.; Entani, S.; Saiki, K.; Koma, A. Atomic and Electronic Structure of CsBr Film Grown on LiF and KBr(001). *Surf. Sci.* **2003**, *523*, 73−79.
(33) Sushko, P. V.; Shluger, A. L.; Catlow, C. R. A. Relative Energies of Surface and Defect States: Ab Initio Calculations of the MgO(001) Surface. *Surf. Sci.* **2000**, *450*, 153−170.
(34) Shluger, A. L.; Sushko, P. V.; Kantorovich, L. V. Spectroscopy of Low-Coordinated Sites: Theoretical Study of MgO. *Phys. Rev. B: Condens. Matter Mater. Phys.* **1999**, *59*, 2417−2430.
(35) Sangster, M. J. L.; Atwood, R. M.; Schroder, U. Interionic Potentials for Alkali Halides. *J. Phys. C: Solid State Phys.* **1978**, *11*, 1523−1540.
(36) Becke, A. D. A. New Mixing of Hartree Fock and Local Density Functional Theories. *J. Chem. Phys.* **1993**, *98*, 5648−5652.
(37) Stephens, P. J.; Devlin, F. J.; Chabalowski, C. F.; Frisch, M. J. Ab Initio Calculation of Vibrational Absorption and Circular Dichroism Spectra Using Density Functional Force Fields. *J. Phys. Chem.* **1994**, *98*, 11623−11627.
(38) Halliday, M. T. E.; Hess, W. P.; Shluger, A. L. Structure and Properties of Electronic and Hole Centers in CsBr from Theoretical Calculations. *J. Phys.: Condens. Matter* **2015**, *27*, 245501−245509.
(39) von Szentpaly, L. V.; Fuentealba, P.; Preuss, H.; Stoll, H. Pseudopotential Calculations on Rb^{2+}, Cs^{2+}, RbH^{+},CsH^{+} and the Mixed Alkali Dimer Ions. *Chem. Phys. Lett.* **1982**, *93*, 555−559.
(40) Hutter, J.; Iannuzzi, M.; Schiffmann, F.; VandeVondele, J. CP2K: Atomistic Simulations of Condensed Matter Systems. *Wiley Interdiscip. Rev. Comp. Mol. Sci.* **2014**, *4*, 15−25.
(41) Adamo, C.; Barone, V. Toward Reliable Density Functional Methods Without Adjustable Parameters: The PBE0Model. *J. Chem. Phys.* **1999**, *110*, 6158−6170.
(42) Adamo, C.; Barone, V. Exchange Functionals with Improved Long-Range Behavior and Adiabatic Connection Methods Without Adjustable Parameters: The mPW and mPW1PW Models. *J. Chem. Phys.* **1998**, *108*, 664−675.
(43) VandeVondele, J.; Hutter, J. Gaussian Basis Sets for Accurate Calculations on Molecular Systems in Gas and Condensed Phases. *J. Chem. Phys.* **2007**, *127*, 114105−114108.
(44) Moellmann, J.; Ehrlich, S.; Tonner, R.; Grimme, S. A DFT-D Study of Structural and Energetic Properties of TiO_2 Modifications. *J. Phys.: Condens. Matter* **2012**, *24*, 424206−424216.
(45) Grimme, S.; Antony, J.; Ehrlich, S.; Krieg, H. A Consistent and Accurate Ab Initio Parametrization of Density Functional Dispersion Correction (DFT-D) for the 94 Elements H-Pu. *J. Chem. Phys.* **2010**, *132*, 154104−154119.
(46) Bruska, M. K.; Czekaj, I.; Delley, B.; Mantzaras, J.; Wokaun, A. Electronic Structure and Oxygen Vacancies in PdO and ZnO: Validation of DFT Models. *Phys. Chem. Chem. Phys.* **2011**, *13*, 15947−15954.
(47) Teegarden, K.; Baldini, G. Optical Absorption Spectra of the Alkali Halides at 10 K. *Phys. Rev.* **1967**, *155*, 896−907.

DOI: 10.1021/acs.jpcc.5b08275
J. Phys. Chem. C 2015, 119, 24036−24045

(48) Gerhardt, U.; Dietz, E. Angular Distribution of Photoelectrons Emitted from Copper Single Crystals. *Phys. Rev. Lett.* **1971**, *26*, 1477−1484.
(49) He, W.; Vilayurganapathy, S.; Joly, A. G.; Droubay, T. C.; Chambers, S. A.; Maldonado, J. R.; Hess, W. P. Comparison of CsBr and KBr Covered Cu Photocathodes: Effects of Laser Irradiation and Work Function Changes. *Appl. Phys. Lett.* **2013**, *102*, 071604.1−071604.5.
(50) Boutboul, T.; Akkerman, A.; Breskin, A.; Chechik, R. Escape Length of Ultraviolet Induced Photoelectrons in Alkali Iodide and CsBr Evaporated Films: Measurements and Modeling. *J. Appl. Phys.* **1998**, *84*, 2890−2896.
(51) Shefer, E.; Breskin, A.; Boutboul, T.; Chechik, R.; Singh, B. K.; Cohen, H.; Feldman, I. Photoelectron Transport in CsI and CsBr Coating Films of Alkali Antimonide and CsI Photocathodes. *J. Appl. Phys.* **2002**, *92*, 4758−4771.
(52) Hess, W. P.; Joly, A. G.; Beck, K. M.; Henyk, M.; Sushko, P. V.; Trevisanutto, P. E.; Shluger, A. L. Laser Control of Desorption Through Selective Surface Excitation. *J. Phys. Chem. B* **2005**, *109*, 19563−19578.
(53) Onodera, Y.; Toyozawa, Y. Excitons in Alkali Halides. *J. Phys. Soc. Jpn.* **1967**, *22*, 833−844.
(54) Kabler, M. N.; Patterson, D. A. Evidence for a Triplet State of the Self-Trapped Exciton in Alkali-Halide Crystals. *Phys. Rev. Lett.* **1967**, *19*, 652−655.
(55) Reed, A. E.; Weinstock, R. B.; Weinhold, F. Natural Population Analysis. *J. Chem. Phys.* **1985**, *83*, 735−746.
(56) Bennewitz, R.; Schaer, S.; Barwich, V.; Pfeiffer, O.; Meyer, E.; Krok, F.; Such, B.; Kolodzej, J.; Szymonski, M. Atomic-Resolution Images of Radiation Damage in KBr. *Surf. Sci.* **2001**, *474*, L197−L202.
(57) Kubo, T.; Okano, A.; Kanasaki, J.; Ishikawa, K.; Nakai, Y.; Itoh, N. Emission of Na atoms from Undamaged and Slightly Damaged NaCl (100) Surfaces by Electronic Excitation. *Phys. Rev. B: Condens. Matter Mater. Phys.* **1994**, *49*, 4931−4937.
(58) Puchin, V. E.; Shluger, A. L.; Itoh, N. The Excitonic Mechanism of Na-atom Desorption from the (100)NaCl Surface. *J. Phys.: Condens. Matter* **1995**, *7*, L147−151.
(59) Franck, J.; Hertz, G. Ueber Zusammenstoesse Zwischen Elektronen und Molekuelen des Quecksilberdampfes und die Ionisierungsspannung desselben. *Verh. Dtsch. Phys. Ges.* **1914**, *16*, 457−467.
(60) Lushchik, A.; Lushchik, C.; Liblik, P.; Maaroos, A.; Makhov, V. N.; Savikhin, F.; Vasil'chenko, E. Luminescent Protection Against Radiation Damage in Wide-Gap Materials. *J. Lumin.* **2009**, *129*, 1894−1897.
(61) Lushchik, A.; Kamada, M.; Kirm, M.; Lushchik, C.; Martinson, I. Direct Excitation of Impurity Centres by Hot Photoelectrons in Ionic Crystals. *Radiat. Meas.* **1998**, *29*, 229−234.
(62) Feldbach, E.; Kamada, M.; Kirm, M.; Lushchik, A.; Lushchik, C.; Martinson, I. Direct Excitation of Tl Impurity Ions by Hot Photoelectrons in Wide-Band Gap Crystals. *Phys. Rev. B: Condens. Matter Mater. Phys.* **1997**, *56*, 13908−13915.
(63) Wilson, J. N.; Curtis, R. M. Dipole Polarizabilities of Ions in Alkali Halide Crystals. *J. Phys. Chem.* **1970**, *74*, 187−196.
(64) McKenna, K. P.; Shluger, A. L. First-Principles Calculations of Defects Near a Grain Boundary in MgO. *Phys. Rev. B: Condens. Matter Mater. Phys.* **2009**, *79*, 224116−224126.
(65) Chowdari, B. V. R.; Itoh, N. Interstitial Halogen Centers in X-Irradiated CsBr. *J. Phys. Chem. Solids* **1972**, *33*, 1773−1783.

DOI: 10.1021/acs.jpcc.5b08275
J. Phys. Chem. C 2015, 119, 24036−24045